

# Efficient geometric integrators for nonadiabatic quantum dynamics in the diabatic basis

Julien Roulet, Seonghoon Choi, and Jiří Vaníček<sup>a)</sup>

*Laboratory of Theoretical Physical Chemistry, Institut des Sciences et Ingénierie Chimiques, Ecole Polytechnique Fédérale de Lausanne (EPFL), CH-1015, Lausanne, Switzerland*

(Dated: 2 April 2022)

The split-operator algorithm combined with the dynamic Fourier method is a popular approach for quantum dynamics in systems with separable kinetic and potential energies because it is explicit, easy to implement, and preserves many geometric invariants of the exact evolution. Although the standard version has only second-order accuracy, it can be recursively symmetrically composed to obtain geometric integrators of arbitrary even order of accuracy in the time step. We have implemented such integrators for nonadiabatic quantum dynamics in the diabatic basis using the triple-jump, Suzuki-fractal, and several non-recursive “optimal” compositions of the second-order split-operator algorithm. Because the automatically generated splitting coefficients are redundant, we reduce the computational cost by pruning these coefficients and lower memory requirements by identifying unique coefficients. The composed integrators are exactly unitary, symplectic, symmetric, time-reversible, and stable regardless of the accuracy of the solution. The order of convergence and preservation of geometric properties are justified analytically and confirmed numerically on a two-surface NaI model in the diabatic representation. Efficiency of higher-order algorithms is sometimes questioned because the number of splitting steps grows exponentially with the order. Yet, we show that, if higher accuracy is desired, higher-order integrators become the most efficient; a 600-fold speedup compared to the second-order split-operator method and a 17000-fold speedup compared to the trapezoidal rule (the Crank-Nicolson method) was observed for convergence error of  $10^{-10}$ .

---

<sup>a)</sup>Electronic mail: jiri.vanicek@epfl.ch

## I. INTRODUCTION

The celebrated Born–Oppenheimer approximation<sup>1,2</sup> assumes the separability of the nuclear and electronic motions in a molecule, and provides an appealing picture of independent electronic potential energy surfaces. However, many important processes in nature<sup>3</sup> can only be described by considering nonadiabatic couplings between these Born–Oppenheimer surfaces.<sup>4–7</sup> To address such processes, one can abandon the Born–Oppenheimer representation and treat electrons and nuclei explicitly,<sup>8–10</sup> use an exact factorization<sup>11,12</sup> of the molecular wavefunction, or, determine which Born–Oppenheimer states are coupled strongly<sup>13,14</sup> and then solve the time-dependent Schrödinger equation with a nonadiabatically coupled molecular Hamiltonian; below, we will only consider the third and most common strategy.

Among various algorithms for nonadiabatic quantum dynamics, *ab initio* multiple spawning<sup>15,16</sup> and related methods, all of which propagate a superposition of Gaussian basis functions along either classical<sup>17,18</sup> or variational<sup>19,20</sup> trajectories, can treat nonadiabatic population dynamics of very large systems. The multiconfigurational time-dependent Hartree (MCTDH) method<sup>21,22</sup> and its multilayer extension<sup>23</sup> are suitable if high accuracy is required and especially if the Hamiltonian can be expressed as a sum of products of one-dimensional operators. The MCTDH and related sparse-grid<sup>24,25</sup> methods owe their efficiency to the fact that only a small fraction of the tensor-product Hilbert space is explored by the quantum dynamics during the time of interest. If the full Hilbert space is accessible, then full grid or time-independent basis sets<sup>25,26</sup> can become more efficient.

As for the molecular Hamiltonian used in nonadiabatic simulations, the *ab initio* electronic structure methods typically yield the *adiabatic* potential energy surfaces, which are nonadiabatically coupled via momentum couplings. However, in the regions of conical intersections,<sup>27,28</sup> the Born–Oppenheimer surfaces become degenerate, and the nonadiabatic couplings diverge. To avoid associated problems, it is convenient to use the diabatic representation, in which the divergent momentum couplings are replaced with well-behaved coordinate couplings. Although exact diabaticization is only possible in systems with two electronic states and one nuclear degree of freedom, there exist more general, approximate diabaticization procedures,<sup>29–31</sup> starting with the vibronic coupling Hamiltonian model.<sup>32</sup> Another benefit of the diabatic representation is that it separates the Hamiltonian into a sum of kinetic energy, depending only on nuclear momenta, and potential energy, depending only

on nuclear coordinates, which makes it possible to propagate the molecular wavefunction with the split-operator algorithm.<sup>25,33,34</sup>

The split-operator algorithm is explicit, easy to implement, and, in addition, it is an example of a geometric integrator<sup>35</sup> because, in contrast to most of the above-mentioned methods, it conserves *exactly* many invariants of the exact solution, regardless of the convergence error of the wavefunction itself. Geometric integrators in general acknowledge special properties of the Schrödinger equation which differentiate it from other differential equations. Using these integrators can be likened to using a well-fitting screw-driver instead of a hammer to attach a screw. Geometric integrators have been very successful in classical molecular dynamics, where the simple Verlet algorithm,<sup>36,37</sup> despite its only second-order accuracy, conserves exactly  $D$  invariants of motion present in every  $D$ -dimensional system, where  $D \sim 10^6$  in state-of-the-art simulations of biomolecules.

The second-order split-operator algorithm<sup>33</sup> is unitary, symplectic, stable, symmetric, and time-reversible, regardless of the size of the time step. However, to obtain highly accurate results, the standard algorithm requires using a small time step, because it has only second-order accuracy. There exist much more efficient algorithms, such as the short-iterative Lanczos algorithm,<sup>38–40</sup> which has an exponential convergence with respect to the time step, and also conserves the norm and energy, but not the inner product (because it is nonlinear) and other geometric properties.

To address the low accuracy of the second-order split-operator algorithm and the nonconservation of geometric properties by other more accurate methods, various higher-order split-operator integrators have been introduced,<sup>41–44</sup> some of which allow complex time steps<sup>44–46</sup> or commutators of the kinetic and potential energies in the exponent,<sup>47–49</sup> thus reducing the number of splitting steps. Here we explore one type of higher-order integrators, designed for nonadiabatic dynamics in the diabatic basis, which we have implemented using the recursive triple-jump<sup>42,43</sup> and Suzuki-fractal,<sup>42</sup> as well as several non-recursive, “optimal” compositions of the second-order split-operator algorithm. While the recursive compositions permit an automated generation of integrators of arbitrary order in the time step,<sup>35,42,43,50,51</sup> the efficiency of higher-order algorithms is sometimes questioned because the number of splitting steps grows exponentially with the order of accuracy, and, consequently, so does the computational cost of a single time step. Motivated by this dilemma, we have explored the convergence and efficiency of the higher-order compositions in detail, concluding that,

despite the increasing number of splittings, the higher-order methods become the most efficient if higher accuracy of the solution is required. We have also confirmed that all composed methods are unitary, symplectic, stable, symmetric, and time-reversible. A final benefit of the higher-order methods is the simple, abstract, and general implementation of the compositions of the second-order split-operator algorithm; indeed, even this “elementary” method is a composition of simpler, first-order algorithms.<sup>25,34</sup> A closely related composition of the first-order explicit and implicit Euler methods yields the second-order trapezoidal rule, which can be also further composed to automatically generate geometric integrators of arbitrary order of accuracy.<sup>52</sup>

The main disadvantage of the split-operator algorithm and its compositions is that their use is restricted to the diabatic representation, in which the Hamiltonian is separable. We, therefore, compare their efficiency with more generally applicable geometric integrators<sup>52</sup> based on composing the trapezoidal rule (the Crank-Nicolson method<sup>53,54</sup>), which can be also used in the adiabatic representation.

The remainder of this paper is organized as follows: In Sec. II, after defining the geometric properties of the exact evolution operator, we discuss the breakdown of time reversibility in the first-order split-operator algorithms and its recovery in the symmetric compositions (proofs are provided in Appendix A). We describe several strategies for reducing the computational cost and memory requirements by pruning redundant splitting coefficients generated automatically by the symmetric compositions. Next, we present the dynamic Fourier method for its ease of implementation and the exponential convergence with the grid density (numerical confirmation provided in Appendix B). For comparison purposes, we briefly review the compositions of trapezoidal rule and implicit midpoint method, which can be used even in the adiabatic basis,<sup>52</sup> but in the diabatic basis are less efficient than the split-operator compositions. In Section III, the convergence properties and conservation of geometric invariants by various methods are analyzed numerically on a two-surface NaI model<sup>55</sup> in the diabatic representation, in which the system has a crossing between two potential energy surfaces. Section IV concludes the paper.

## II. THEORY

In this section, we follow closely the structure of Section II of Ref. 52. The time-dependent Schrödinger equation

$$i\hbar \frac{d\psi(t)}{dt} = \hat{H}\psi(t) \quad (1)$$

with a time-independent Hamiltonian  $\hat{H}$  and initial condition  $\psi(0)$  has the formal solution  $\psi(t) = \hat{U}(t)\psi(0)$ , where  $\hat{U}(t)$  is the evolution operator. The exact evolution operator

$$\hat{U}_{\text{ex}}(t) = e^{-i\hat{H}t/\hbar} \quad (2)$$

is linear, time-reversible, stable, and conserves both the norm of the quantum state and expectation value of its energy. Because these properties are desirable also in approximate numerical evolution operator  $\hat{U}_{\text{appr}}(t)$ , let us define and discuss them in more detail.

### A. Geometric properties of the exact evolution operator

A norm of a vector  $\psi$  in a Hilbert space is the non-negative real number  $\|\psi\| := \langle \psi | \psi \rangle^{1/2}$ , where  $\langle \psi | \phi \rangle$  denotes the inner product. An operator  $\hat{U}$  is said to *preserve the norm* if  $\|\hat{U}\psi\| = \|\psi\|$  for all  $\psi$ , and to *preserve the inner product* if

$$\langle \hat{U}\psi | \hat{U}\phi \rangle = \langle \psi | \phi \rangle \quad (3)$$

for all  $\psi$  and  $\phi$ . For linear operators  $\hat{U}$ , these two properties are equivalent, whereas for general, possibly nonlinear operators, conservation of the inner product implies linearity<sup>56</sup> and conservation of norm, but norm conservation implies neither linearity nor conservation of the inner product. The *Hermitian adjoint* of operator  $\hat{A}$  is an operator  $\hat{A}^\dagger$  such that  $\langle \psi | \hat{A}\phi \rangle \equiv \langle \hat{A}^\dagger\psi | \phi \rangle$  for all  $\psi, \phi$ . The preservation of inner product is, therefore, equivalent to the condition that

$$\hat{U}^\dagger \hat{U} = 1. \quad (4)$$

Such an operator  $\hat{U}$  is said to be *unitary*. The exact evolution operator is unitary because  $\hat{U}_{\text{ex}}(t)^\dagger = \exp(i\hat{H}t/\hbar) = \hat{U}_{\text{ex}}(t)^{-1}$ .

A *symplectic two-form*  $\omega(\psi, \phi)$  is any nondegenerate skew-symmetric bilinear form on a vector space. An operator  $\hat{U}$  is called *symplectic* if  $\omega(\hat{U}\psi, \hat{U}\phi) = \omega(\psi, \phi)$ . Throughout this paper, we will consider the symplectic two-form defined as<sup>25</sup>

$$\omega(\psi, \phi) := -2\hbar \text{Im} \langle \psi | \phi \rangle; \quad (5)$$

obviously, it is conserved if the inner product  $\langle\psi|\phi\rangle$  itself is. The exact evolution operator is therefore symplectic.

Let  $\langle\hat{A}\rangle_{\psi(t)} := \langle\psi(t)|\hat{A}|\psi(t)\rangle$  denote the expectation value of operator  $\hat{A}$  in the state  $\psi(t)$ . It is easy to see that the *energy* is conserved if the evolution operator is unitary and commutes with the Hamiltonian

$$\begin{aligned} E(t) &= \langle\hat{H}\rangle_{\psi(t)} := \langle\psi(t)|\hat{H}|\psi(t)\rangle \\ &= \langle\psi(0)|\hat{U}(t)^\dagger\hat{H}\hat{U}(t)|\psi(0)\rangle \\ &= \langle\psi(0)|\hat{U}(t)^\dagger\hat{U}(t)\hat{H}|\psi(0)\rangle \\ &= \langle\psi(0)|\hat{H}|\psi(0)\rangle = E(0). \end{aligned} \tag{6}$$

Because it is unitary and commutes with  $\hat{H}$ , the exact evolution conserves energy.

An *adjoint*  $\hat{U}(t)^*$  of an evolution operator  $\hat{U}(t)$  is defined as

$$\hat{U}(t)^* := \hat{U}(-t)^{-1}. \tag{7}$$

An evolution operator is said to be *symmetric* if<sup>35</sup>

$$\hat{U}(t)^* = \hat{U}(t) \tag{8}$$

and *time-reversible* if<sup>35</sup> the forward and backward evolutions for time  $t$  cancel each other exactly:

$$\hat{U}(-t)\hat{U}(t)\psi(0) = \psi(0). \tag{9}$$

Time reversibility is, therefore, a direct consequence of symmetry. The exact evolution operator is both symmetric and time-reversible because  $\hat{U}_{\text{ex}}(t)^* = \exp(-i\hat{H}t/\hbar)$ .

As for the stability, the time evolution is called:

(i) *stable*<sup>57–59</sup> if for every  $\epsilon > 0$ , there is  $\delta(\epsilon) > 0$  such that

$$\|\psi(0) - \phi(0)\| < \delta \text{ implies } \|\psi(t) - \phi(t)\| < \epsilon \text{ for all } t; \tag{10}$$

(ii) *attracting*<sup>57,59</sup> if there is a  $\delta > 0$  such that

$$\|\psi(0) - \phi(0)\| < \delta \text{ implies } \|\psi(t) - \phi(t)\| \rightarrow 0 \text{ as } t \rightarrow \infty; \tag{11}$$

(iii) *asymptotically stable* if it is both stable and attracting.

For a pictorial representation of these conditions, see Fig. 1 of Ref. 52. Due to its unitarity, the exact evolution is stable but not asymptotically stable:

$$\|\psi(t) - \phi(t)\| = \|\psi(0) - \phi(0)\|. \tag{12}$$

## B. First-order split-operator methods

In approximate propagation methods, the state at time  $t + \Delta t$  is obtained from the state at time  $t$  using the relation

$$\psi(t + \Delta t) = \hat{U}_{\text{appr}}(\Delta t)\psi(t)$$

where  $\hat{U}_{\text{appr}}(\Delta t)$  is an approximate time evolution operator and  $\Delta t$  the numerical time step. Depending on the order of kinetic and potential propagations, the approximate evolution operator is

$$\hat{U}_{\text{VT}}(\Delta t) := e^{-\frac{i}{\hbar}\Delta t\hat{V}}e^{-\frac{i}{\hbar}\Delta t\hat{T}} \quad (13)$$

in the *VT split-operator algorithm* and

$$\hat{U}_{\text{TV}}(\Delta t) := e^{-\frac{i}{\hbar}\Delta t\hat{T}}e^{-\frac{i}{\hbar}\Delta t\hat{V}} \quad (14)$$

in the *TV split-operator algorithm*. Both are unitary, symplectic, stable, and first-order in the time step  $\Delta t$ . Neither method conserves energy because neither evolution operator commutes with the Hamiltonian. Neither method is symmetric; in fact, they are adjoints of each other. Hence, neither method is time-reversible. These properties are justified in Appendix A and summarized in Table I.

Although the first-order split-operator algorithms are not time-reversible, composing them in a specific way leads to time-reversible integrators of arbitrary order of accuracy in the time step.

TABLE I. Geometric properties and computational cost of the first-order and recursively composed second-order split-operator (SO) algorithms. Cost (here before speedup by pruning splitting coefficients) is measured by the number of fast Fourier transforms required per time step (see Sec. II G).  $n$  is the number of recursive compositions and  $C$  the total number of composition steps per time step ( $C = 3^n$  for the triple jump<sup>42,43</sup>,  $C = 5^n$  for Suzuki's fractal<sup>42</sup>). + or - denotes that the geometric property of the exact evolution operator is or is not preserved.

Method	Order	Unitary	Symplectic	Commutates with $\hat{H}$	Energy cons.	Symm- etric	Time- reversible	Stable	Cost
1 <sup>st</sup> order SO	1	+	+	-	-	-	-	+	2
2 <sup>nd</sup> order SO	$2(n+1)$	+	+	-	-	+	+	+	$2C$

### C. Recovery of geometric properties by composed methods

Composing the two first-order split-operator algorithms, each for a time step  $\Delta t/2$ , yields a symmetric second-order method.<sup>33</sup> Depending on the order of composition, one obtains either the *VTV algorithm*

$$\hat{U}_{\text{VTV}}(\Delta t) := \hat{U}_{\text{VT}}(\Delta t/2)\hat{U}_{\text{TV}}(\Delta t/2), \quad (15)$$

or *TVT algorithm*

$$\hat{U}_{\text{TVT}}(\Delta t) := \hat{U}_{\text{TV}}(\Delta t/2)\hat{U}_{\text{VT}}(\Delta t/2). \quad (16)$$

Both are explicit, unitary, symplectic, stable, symmetric, and time-reversible, regardless of the size of the time step. Neither evolution operator commutes with the Hamiltonian and, therefore, neither method conserves energy exactly. These properties are again justified in Appendix A and summarized in Table I.

### D. Symmetric composition schemes for symmetric methods

Composing any symmetric second-order methods (such as those of Sec. II C) with appropriately chosen time steps leads to symmetric integrators of arbitrary order of accuracy.<sup>35,42,43</sup> Indeed, there are a natural number  $M$  and real numbers  $\gamma_n$ ,  $n = 1, \dots, M$ , called *composition coefficients*, such that  $\gamma_1 + \dots + \gamma_M = 1$  and such that for any symmetric evolution operator  $\hat{U}_p(\Delta t)$  of an even order  $p$ ,

$$\hat{U}_{p+2}(\Delta t) := \hat{U}_p(\gamma_M \Delta t) \cdots \hat{U}_p(\gamma_1 \Delta t)$$

is a symmetric integrator of order  $p + 2$ . The simplest composition schemes (see Fig. 2 of Ref. 52) are the triple jump<sup>41–43,60</sup> with  $M = 3$ ,

$$\gamma_1 = \frac{1}{2 - 2^{1/(p+1)}}, \quad \gamma_2 = -\frac{2^{1/(p+1)}}{2 - 2^{1/(p+1)}}, \quad (17)$$

and Suzuki's fractal<sup>42</sup> with  $M = 5$ ,

$$\gamma_1 = \gamma_2 = \frac{1}{4 - 4^{1/(p+1)}}, \quad \gamma_3 = -\frac{4^{1/(p+1)}}{4 - 4^{1/(p+1)}}. \quad (18)$$

Both are *symmetric compositions*, meaning that the remaining coefficients are obtained from the relation  $\gamma_{M+1-n} = \gamma_n$ .



Although the  $p^{\text{th}}$ -order integrator obtained using Suzuki's fractal requires  $(5/3)^{\frac{p}{2}-1}$  times more composition steps than the integrator obtained from the same symmetric second-order method using the triple jump, larger time steps can be used for calculations using Suzuki's fractal, and, therefore, Suzuki-fractal composition is sometimes more efficient (see Ref. 52 for a numerical example). Even more efficient non-recursive composition schemes exist for specific orders. These "optimal" composition schemes were implemented according to Kahan and Li<sup>61</sup> for the 6<sup>th</sup> and 8<sup>th</sup> orders, and according to Sofroniou and Spaletta<sup>62</sup> for the 10<sup>th</sup> order (see Fig. 2 of Ref. 52).

### E. Compositions of split-operator algorithms

The split-operator algorithm is applicable if the Hamiltonian  $\hat{H}$  can be written as a sum

$$\hat{H} = \hat{A} + \hat{B} \quad (19)$$

of operators  $\hat{A}$  and  $\hat{B}$  with evolution operators,  $\hat{U}_{\hat{A}}(t) = \exp(-it\hat{A}/\hbar)$  and  $\hat{U}_{\hat{B}}(t) = \exp(-it\hat{B}/\hbar)$ , whose actions on  $\psi$  can be evaluated exactly. A general split-operator evolution operator can be expressed as

$$\hat{U}_{\hat{A}+\hat{B}}^{\text{SO}}(\Delta t) = \hat{U}_{\hat{B}}(b_N\Delta t)\hat{U}_{\hat{A}}(a_N\Delta t)\cdots\hat{U}_{\hat{B}}(b_1\Delta t)\hat{U}_{\hat{A}}(a_1\Delta t),$$

where  $N$  is the number of splitting steps, and  $a_j$  and  $b_j$  are the splitting coefficients associated with the operators  $\hat{A}$  and  $\hat{B}$ . These coefficients in general satisfy the identity  $\sum_{j=1}^N a_j = \sum_{j=1}^N b_j = 1$ , and are  $a_1 = b_1 = 1$  for the first-order VT and TV algorithms<sup>63</sup> and

$$a_1 = a_2 = \frac{1}{2}, \quad b_1 = 1, \quad b_2 = 0 \quad (20)$$

for the second-order VTV or TVT algorithms.<sup>64</sup>

Because the second-order split-operator algorithm<sup>64</sup> is symmetric, it can be composed by any of the composition schemes discussed in Sec. II D. For example, the splitting coefficients of a fourth-order method are

$$\begin{aligned} a_1 = a_2 &= \frac{1}{2(2 - 2^{1/3})}, & a_3 &= -\frac{2^{1/3}}{2(2 - 2^{1/3})}, \\ b_1 &= \frac{1}{2 - 2^{1/3}}, & b_3 &= -\frac{2^{1/3}}{2 - 2^{1/3}}, & b_2 = b_6 &= 0 \end{aligned} \quad (21)$$

with  $N = 6$  if the triple-jump composition scheme is used, and

$$\begin{aligned} a_1 = a_2 = a_3 = a_4 &= \frac{1}{2(4 - 4^{1/3})}, & a_5 &= -\frac{4^{1/3}}{2(4 - 4^{1/3})}, \\ b_1 = b_3 &= \frac{1}{4 - 4^{1/3}}, & b_2 = b_4 = b_{10} &= 0, & b_5 &= -\frac{4^{1/3}}{4 - 4^{1/3}} \end{aligned} \quad (22)$$

with  $N = 10$  if Suzuki's fractal is used instead. The remaining coefficients are obtained from symmetry as

$$a_{N-j+1} = a_j, \quad b_{N-j} = b_j. \quad (23)$$

Both composition procedures can be applied recursively to obtain higher-order split-operator algorithms (see Fig. 1).

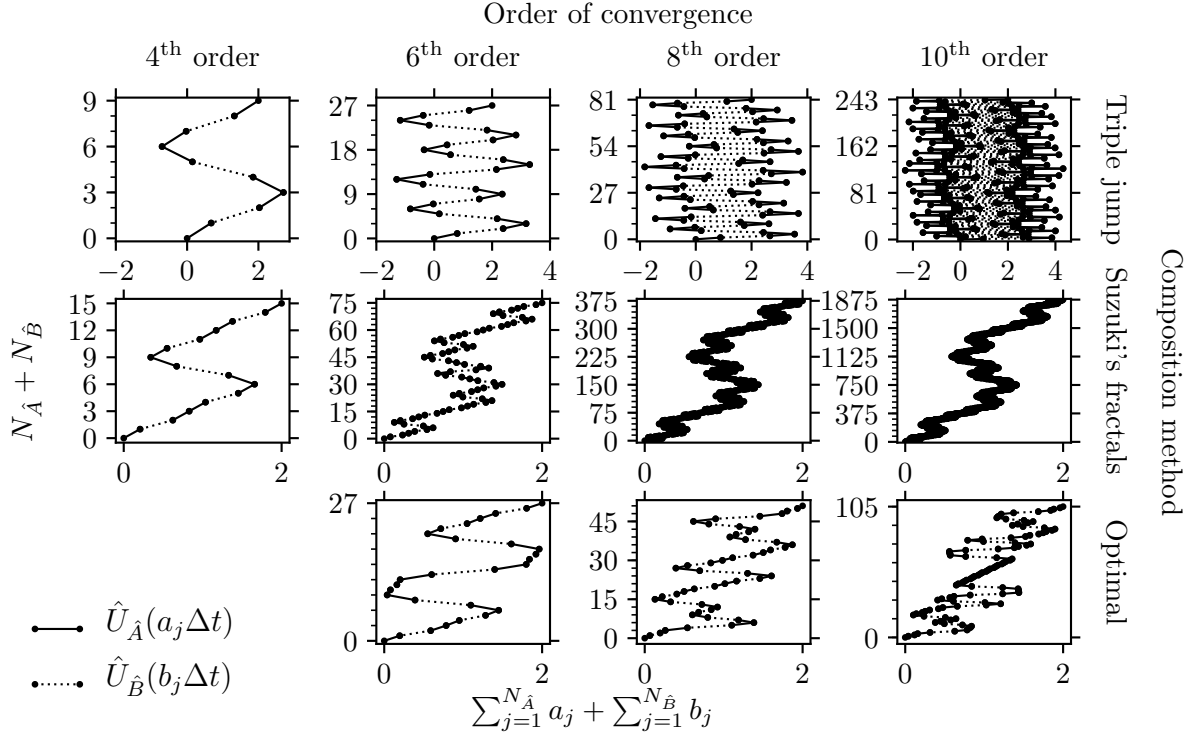


FIG. 1. Split-operator algorithms composed by the recursive (triple jump and Suzuki's fractal) and nonrecursive “optimal” composition schemes.  $N_{\hat{O}}$  is the number of actions of  $\hat{U}_{\hat{O}}$  on  $\psi$ .

All compositions of the second-order VTV or TVT split-operator algorithms are unitary, symplectic, and stable; all symmetric compositions are symmetric and therefore time-reversible. The proof of this statement is a special case of the general proof of a corresponding theorem for the composition of geometric integrators in Ref. 52.

## F. Pruning splitting coefficients

Many  $b_j$  coefficients of the higher-order integrators obtained by recursive composition of the second-order split-operator algorithm are zero [see Eqs. (21) and (22)]. The computational time can be reduced by “pruning,” i.e., removing the splitting steps corresponding to  $b_j = 0$  and merging the consecutive actions of  $\hat{U}_{\hat{A}}(a_j\Delta t)$  and  $\hat{U}_{\hat{A}}(a_{j+1}\Delta t)$ . If  $b_j = 0$  and  $j \neq N$ , the splitting coefficients are modified as

$$\begin{aligned}\tilde{b}_k &= b_{k+1}, \quad \text{for } j \leq k \leq N-1, \\ \tilde{a}_j &= a_j + a_{j+1}, \\ \tilde{a}_k &= a_{k+1}, \quad \text{for } j+1 \leq k \leq N-1,\end{aligned}\tag{24}$$

$$\tilde{N} = N - 1,\tag{25}$$

in order to merge the  $j^{\text{th}}$  and  $(j+1)^{\text{th}}$  steps. The composed methods after the merge are exhibited in Fig. 2 and the reduction in the number  $N$  of splitting steps, which measures the computational cost, is summarized in Table II.

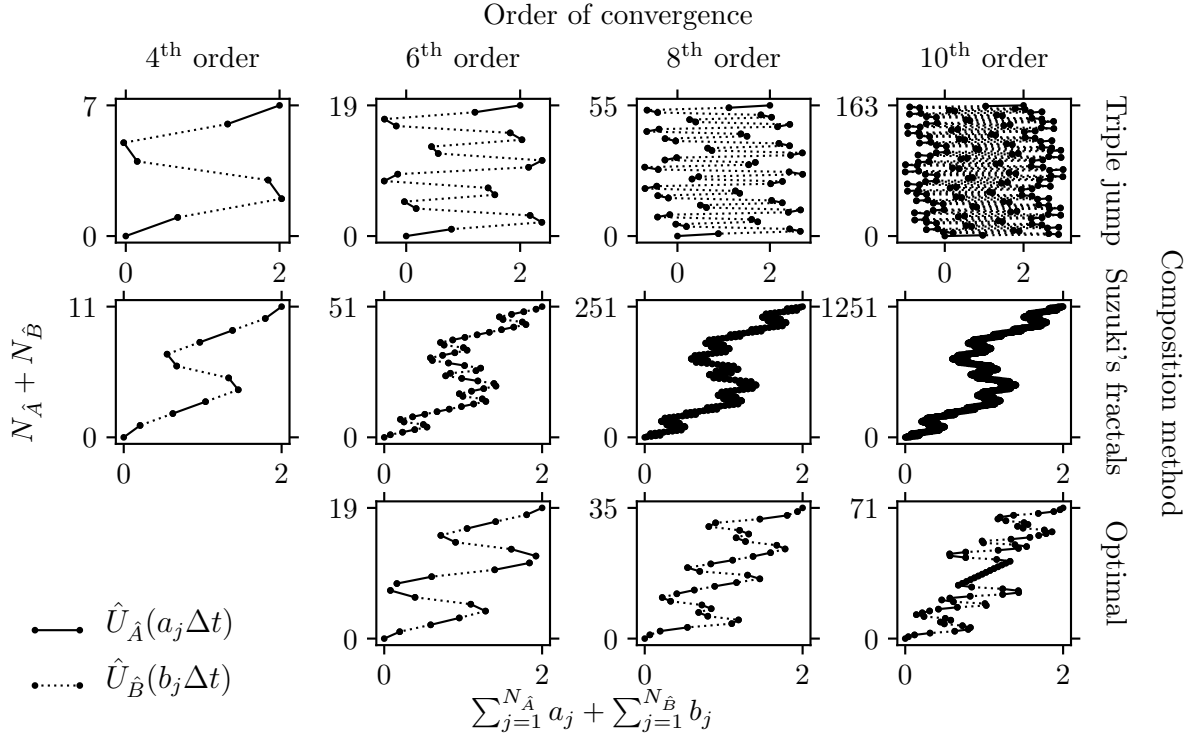


FIG. 2. Composed split-operator algorithms from Fig. 1 after removing zero splitting coefficients and merging adjacent coefficients.

For a time-independent separable Hamiltonian, one can either precompute and store the evolution operators,  $\hat{U}_{\hat{A}}(a_j\Delta t)$  and  $\hat{U}_{\hat{B}}(b_j\Delta t)$ , or compute them on the fly. The former approach is more memory intensive than the latter, which does not store any evolution operators, but the computational time is reduced since the evolution operators are only computed once at initialization. To alleviate the memory requirement of the former approach, one can exploit the repetition of certain splitting coefficients, which is obvious from Eqs. (21) and (22) and Fig. 2. If either  $\hat{A}$  or  $\hat{B}$  is time-dependent, it is always beneficial to compute the evolution operator pertaining to the time-dependent operator on the fly because no reduction in computational time is possible by precomputing the evolution operators.

The effort spent in searching for repeated coefficients is reduced if the symmetries of the composition scheme and of the elementary method are exploited [see Eq. (23)]. The repeated coefficients are then identified from only half of the original coefficients  $a_j$  and  $b_j$ .

Once identified, only the unique evolution operators  $\hat{U}_{\hat{A}}(a_j^{\text{uniq}}\Delta t)$  and  $\hat{U}_{\hat{B}}(b_j^{\text{uniq}}\Delta t)$  are stored in arrays of lengths  $N_a^{\text{uniq}}$  and  $N_b^{\text{uniq}}$ , together with the information when to apply them, stored in integer arrays  $I^a$  and  $I^b$  of length  $N$ , containing the indices in unique coefficient arrays, i.e.,

$$1 \leq I_j^a \leq N_a^{\text{uniq}}, \quad 1 \leq I_j^b \leq N_b^{\text{uniq}}. \quad (26)$$

Exploiting the repeated coefficients, the number of stored evolution operators reduces from  $2N$  to  $N_a^{\text{uniq}} + N_b^{\text{uniq}}$  (see Table II).

## G. Dynamic Fourier method and molecular Hamiltonian in the diabatic basis

To propagate a wavepacket  $\psi(t)$  with any split-operator algorithm (see Secs. II B–II D), only the actions of the kinetic ( $\hat{U}_{\hat{T}}$ ) and potential ( $\hat{U}_{\hat{V}}$ ) evolution operators on  $\psi(t)$  are required, where

$$\hat{U}_{\hat{T}}(\Delta t) := e^{-i\frac{\Delta t}{\hbar}\hat{T}} \text{ and } \hat{U}_{\hat{V}}(\Delta t) := e^{-i\frac{\Delta t}{\hbar}\hat{V}}.$$

The dynamic Fourier method<sup>33,34,65,66</sup> provides an efficient way of computing  $f(\hat{X})\psi(t)$  for an arbitrary function  $f(\hat{X})$ , where  $\hat{X}$  is either the nuclear position ( $\hat{Q}$ ) or momentum ( $\hat{P}$ ) operator. Each action of  $f(\hat{X})$  on  $\psi(t)$  is implemented in the  $X$ -representation, in which  $\hat{X}$  is diagonal, via a simple pointwise multiplication, after Fourier-transforming  $\psi(t)$  to change the representation if necessary. In the numerical examples below, the Fourier transform was performed using the Fastest Fourier Transform in the West 3 (FFTW3) library.<sup>67</sup> Although

its accuracy is sufficient for most applications, small deviations from unitarity, which were due to the high number of repeated application of the forward and backward Fourier transforms, affected the most converged calculations. To reduce the nonunitarity, we used the long-double instead of the default double precision version of FFTW3.

The molecular Hamiltonian in the diabatic basis can be expressed as

$$\hat{\mathbf{H}} = \frac{1}{2} \hat{\mathbf{P}}^T \cdot \mathbf{M}^{-1} \cdot \hat{\mathbf{P}} \mathbf{1} + \mathbf{V}(\hat{\mathbf{Q}}), \quad (27)$$

where  $\mathbf{M}$  is the diagonal  $D \times D$  nuclear mass matrix,  $D$  the number of nuclear degrees of freedom, and  $\mathbf{V}$  the potential energy. In Eq. (27), the dot  $\cdot$  denotes the matrix product in nuclear  $D$ -dimensional vector space, the hat  $\hat{\cdot}$  represents a nuclear operator, and the

TABLE II. Computational cost and memory requirement of the composed split-operator algorithms before and after pruning (i.e., removing zero coefficients and merging adjacent coefficients) and identifying repeated coefficients. The computational cost is measured by  $N_{\hat{A}} + N_{\hat{B}}$ , where  $N_{\hat{O}}$  is the number of actions of  $\hat{U}_{\hat{O}}$  on the wavepacket. The memory requirement before and after pruning is  $N_{\hat{A}} + N_{\hat{B}}$ , and after identifying repeated coefficients decreases to  $N_{\hat{A}}^{\text{unq}} + N_{\hat{B}}^{\text{unq}}$ .

Composition	Order	$N_{\hat{A}} + N_{\hat{B}}$	$N_{\hat{A}} + N_{\hat{B}}$	$N_a^{\text{unq}}$	$N_b^{\text{unq}}$
method		before merge	after merge		
Elementary methods	1	2	2	1	1
	2	3	3	1	1
Triple jump	4	9	7	2	2
	6	27	19	4	4
	8	81	55	8	8
	10	243	163	16	16
Suzuki's fractal	4	15	11	3	2
	6	75	51	6	4
	8	375	251	12	8
	10	1875	1251	24	16
Optimal	6	27	19	5	5
	8	51	35	9	9
	10	105	71	18	18

bold font indicates an electronic operator, i.e., an  $S \times S$  matrix, where  $S$  is the number of included electronic states. Using the dynamic Fourier method, each evaluation of the action of the pair  $\hat{\mathbf{U}}_{\mathbf{V}}(t_V)$  and  $\hat{\mathbf{U}}_{\mathbf{T}}(t_T)$  on a molecular wavepacket  $\psi(t)$ , which now becomes an  $S$ -component vector of nuclear wavepackets (one on each surface), involves two changes of the wavepacket's representation. The above-mentioned nonunitarity of the solution, partially due to the numerical implementation of the FFT algorithm, was made worse by the matrix exponential required for evaluating the potential evolution operator  $\hat{\mathbf{U}}_{\mathbf{V}}(t_V)$ , which contains offdiagonal couplings between the electronic states. Although we tried different approaches for matrix exponentiation, including Padé approximants<sup>68,69</sup> and exponentiating a diagonal matrix obtained with the QR decomposition<sup>68,70</sup> or with the Jacobi method,<sup>68</sup> none of the three methods was better than the others in reducing the nonunitarity. Because the Jacobi method is exact after one iteration for  $2 \times 2$  matrices, it was used for all results in Section III.

## H. Trapezoidal rule and implicit midpoint method

In addition to nonconservation of energy, the main disadvantage of the split-operator algorithms is that they can be applied for nonadiabatic dynamics only in the diabatic representation. Yet, there exist closely related, arbitrary-order geometric integrators,<sup>52</sup> which, in addition, conserve energy and are applicable both in the diabatic and adiabatic representations. These integrators are, like the higher-order split-operator algorithms, based on recursive symmetric composition (see Sec. II D) of the second-order trapezoidal rule (Crank-Nicolson method<sup>53,54</sup>) or the implicit midpoint method

$$\hat{U}_{\text{trap}}(\Delta t) := \hat{U}_{\text{impl}}(\Delta t/2)\hat{U}_{\text{expl}}(\Delta t/2), \quad (28)$$

$$\hat{U}_{\text{midp}}(\Delta t) := \hat{U}_{\text{expl}}(\Delta t/2)\hat{U}_{\text{impl}}(\Delta t/2), \quad (29)$$

both of which are, themselves, compositions of the explicit and implicit Euler methods

$$\hat{U}_{\text{expl}}(\Delta t) := 1 - \frac{i}{\hbar}\Delta t \hat{H}, \quad (30)$$

$$\hat{U}_{\text{impl}}(\Delta t) := \left(1 + \frac{i}{\hbar}\Delta t \hat{H}\right)^{-1}. \quad (31)$$

Due to the presence of implicit steps, the trapezoidal rule, implicit midpoint method as well as their compositions require solving large, although sparse, linear systems iteratively,<sup>52</sup> and, as a result, in the diabatic representation are expected to be significantly less efficient

than the explicit split-operator algorithms of the same order of accuracy. All compositions of the trapezoidal rule and implicit midpoint method are unitary, symplectic, energy-conserving, and stable, but only the symmetric compositions are symmetric and, therefore, time-reversible. Equations (30)-(31) show that these integrators are most naturally implemented in conjunction with the dynamic Fourier method described in Sec. II G; the only difference being that one must evaluate the operation  $(\hat{T} + \hat{V})\psi$  instead of  $\hat{U}_{\hat{T}}\psi$  and  $\hat{U}_{\hat{V}}\psi$ .

### III. NUMERICAL EXAMPLES

To test the geometric and convergence properties of the split-operator algorithms presented in Sections II B–II D, we used these integrators to simulate the nonadiabatic quantum dynamics in a one-dimensional two-surface model<sup>55</sup> of the NaI molecule, motivated by the experiment by Mokhtari *et al.*<sup>3</sup>

Before the electronic excitation, the NaI molecule was assumed to be in the ground vibrational eigenstate of a harmonic fit to the ground-state potential energy surface at the equilibrium geometry. Assuming the validity of the Condon approximation and time-dependent perturbation theory, this vibrational wavepacket was then promoted to the excited-state surface, in order to obtain an initial Gaussian wavepacket ( $q_0 = 4.9889$  a.u.,  $p_0 = 0.0$  a.u.,  $\sigma_0 = 0.110436$  a.u.) for the nonadiabatic dynamics, performed by solving the time-dependent Schrödinger equation exactly. The top panel of Fig. 3 shows the two diabatic potential energy surfaces as well as the initial wavepacket at  $t = 0$  and the ground- and excited-state components of the final wavepacket at the final time  $t_f = 10500$  a.u.; a long-enough propagation time was chosen so that the wavepacket traverses the crossing between the diabatic surfaces. The population dynamics of NaI, displayed in the middle and bottom panels of Fig. 3, shows that after passing this crossing, most of the population jumps to the other diabatic state, while a small fraction remains in the original, dissociative diabatic state. The figure also confirms that the converged populations obtained with different integrators agree on the scale visible in the figure. In particular, the results obtained with the VTV and TVT split-operator algorithms agree with each other and also with the results of the trapezoidal and midpoint rule (middle panel). Also the results of the triple-jump, Suzuki-fractal, and optimal compositions of the second-order VTV algorithm agree with each other (bottom panel).

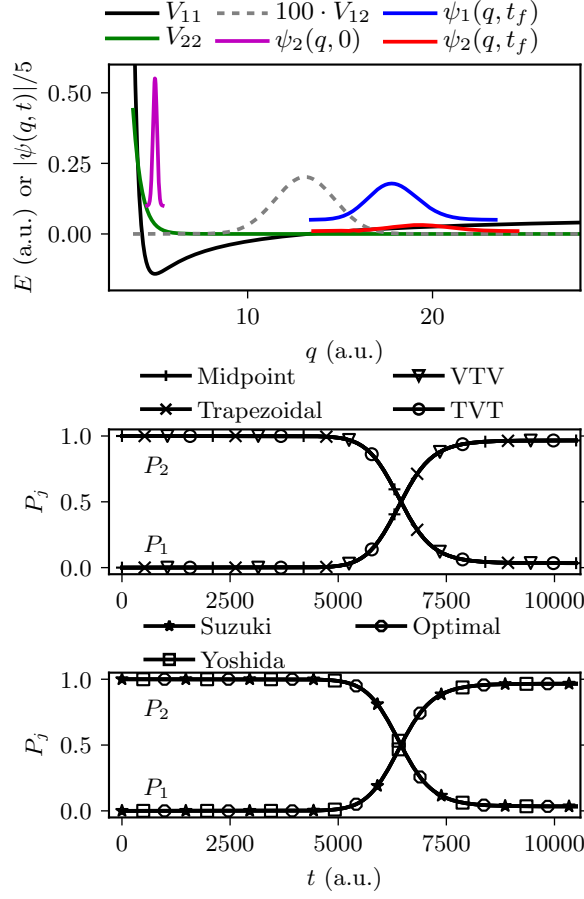


FIG. 3. Nonadiabatic dynamics of NaI. Top: Diabatic potential energy surfaces with the initial and final nuclear wavepacket components in the two diabatic electronic states. Middle: Populations of NaI in the two diabatic states computed with four different second-order methods. Bottom: Populations computed with three different sixth-order compositions of the VTV algorithm. Populations were propagated with a time step  $\Delta t = 0.01$  a.u. for the second-order methods and  $\Delta t = 82.03125$  a.u. for the sixth-order methods, i.e., much more frequently than the markers suggest. The time step guaranteed wavepacket convergence errors below  $\approx 10^{-5}$  in all methods.

For a quantitative comparison of various algorithms, it is necessary to compare their convergence errors at the final time  $t_f$ . In our setting, the convergence error at time  $t$  is defined as the  $L_2$ -norm error  $\|\psi_{\Delta t}(t) - \psi_{\Delta t/2}(t)\|$ , where  $\psi_{\Delta t}(t)$  denotes the wavepacket propagated with a time step  $\Delta t$ . Figure 4 plots the convergence error as a function of the time step and confirms, for each algorithm, the asymptotic order of convergence predicted in Sections II B–II D. For clarity, in this and all remaining figures, only the VT algorithm and compositions of the VTV algorithm are compared because the corresponding results



of the TV algorithm and compositions of the TVT algorithms behave similarly. The top panel of Fig. 4 compares all methods, whereas the bottom left-hand panel compares only the different orders of the triple-jump composition and the bottom right-hand panel different composition schemes with the sixth-order convergence. It is clear that, for a given order of convergence, the prefactor of the error is the largest for the triple-jump,<sup>42,43</sup> intermediate for the optimal,<sup>61</sup> and smallest for Suzuki-fractal composition. The figure also shows that for the smallest time steps, the error starts to increase again. This is due to the accumulating numerical error of the fast Fourier transform, which eventually outweighs the error due to time discretization. As a result, the predicted asymptotic order of convergence cannot be observed for some methods because it is only reached for very small time steps.

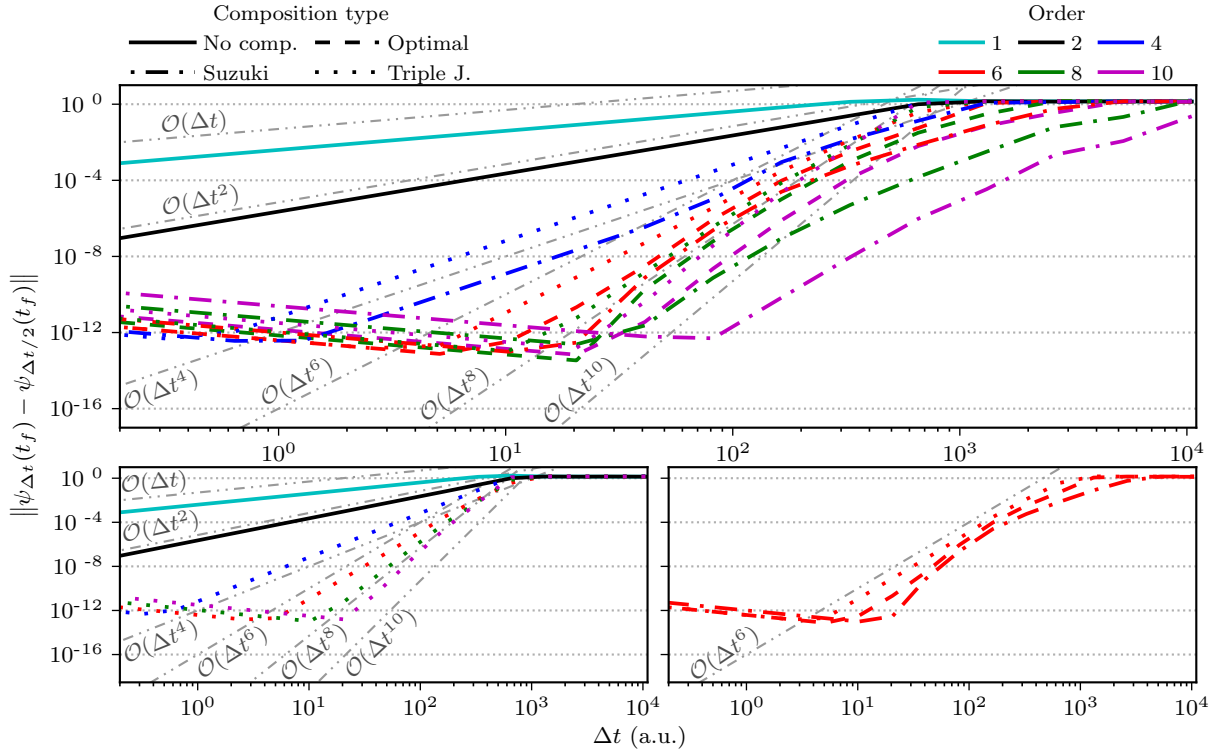


FIG. 4. Convergence of the molecular wavefunction as a function of the time step. Gray lines were added to guide the eye. Top: all discussed methods, bottom left: methods composed with the triple-jump scheme, bottom right: sixth-order methods.

Efficiency of an algorithm is not determined solely by the convergence error for a given time step  $\Delta t$  because the number of composition steps depends on the composition scheme and, in addition, for the recursive schemes, grows exponentially with the order of conver-

gence. Figure 5 therefore displays the wavefunction convergence error of each algorithm as a function of the computational (CPU) time. Comparison of the compositions of the VTV split-operator algorithm in the top panel of Fig. 5 shows that the fourth-order Suzuki composition takes less CPU time already to achieve convergence error  $10^{-2}$  than does the elementary VTV algorithm. To reach errors below  $10^{-2}$ , it is more efficient to use some of the fourth or higher-order integrators. Remarkably, the CPU time required to reach an error of  $10^{-10}$  is roughly 600 times longer for the basic VTV algorithm than for its optimal 6<sup>th</sup>-order composition. The bottom right-hand panel of Fig. 5 confirms the prediction that the optimal compositions are the most efficient among composition methods of the same order.

Convergence curves in Figs. 4 and 5 were obtained using the long-double precision for the FFTW3 algorithm, which lowered the error accumulation resulting from the nonunitarity of the FFTW3 Fourier transform. If high accuracy is not desired, the double precision of the FFTW3 algorithm can be used instead, resulting in much more efficient higher-order algorithms. This is shown in Fig. 6, which compares the efficiency of the Suzuki compositions of the VTV algorithm evaluated either with the double or long-double implementation of the FFTW3, and also with the corresponding compositions of the trapezoidal rule (for which the double precision of FFTW3 was sufficient). Even the more expensive, long-double precision calculation with the compositions of VTV algorithm are faster than the corresponding double precision calculations with the trapezoidal rule, which requires an expensive iterative solution of a system of linear equations. In particular, to reach a convergence error of  $10^{-10}$ , a 20-fold speedup is achieved by using the sixth-order Suzuki-fractal composition of the VTV algorithm instead of the same composition of the trapezoidal rule (see Fig. 6), and a 17000-fold speedup by using the optimally composed sixth-order VTV algorithm instead of the elementary trapezoidal rule (see Figs. 5 and 6). Note that the dependence of CPU time on the error in Fig. 6 is not monotonous for the compositions of the trapezoidal rule because the convergence of the numerical solution to the system of linear equations required more iterations for larger time steps; as a result, both the error and CPU time increased for time steps larger than a certain critical value.

To check that the increased efficiency of higher-order compositions is not achieved by sacrificing the conservation of geometric invariants, we analyzed the conservation of norm, symplectic two-form, energy, and time reversibility. Conservation of the norm and symplectic

two-form, and nonconservation of energy by all split-operator algorithms is demonstrated in panels (a)-(c) of Fig. 7. The tiny residual errors ( $< 10^{-12}$  in all cases) result from accumulated numerical errors of the FFT and matrix exponentiation (see Sec. II G). Panels (d) and (e) confirm, on one hand, that the first-order split-operator algorithm is not time-reversible, and, on the other hand, that the second-order VTV algorithm together with all its compositions are exactly time-reversible; the tiny residual errors are again due to accumulated numerical errors of the FFT and matrix exponentiation.

The nonconservation of energy by the split-operator algorithms is further inspected in Fig. 8, showing the error of energy as the function of the time step. For the Suzuki-fractal compositions of the VTV algorithm, the energy is only conserved approximately; its conservation follows the order of convergence of the integrator, as indicated by the gray lines. In contrast, the trapezoidal rule conserves the energy to machine accuracy, regardless of the size of the time step.

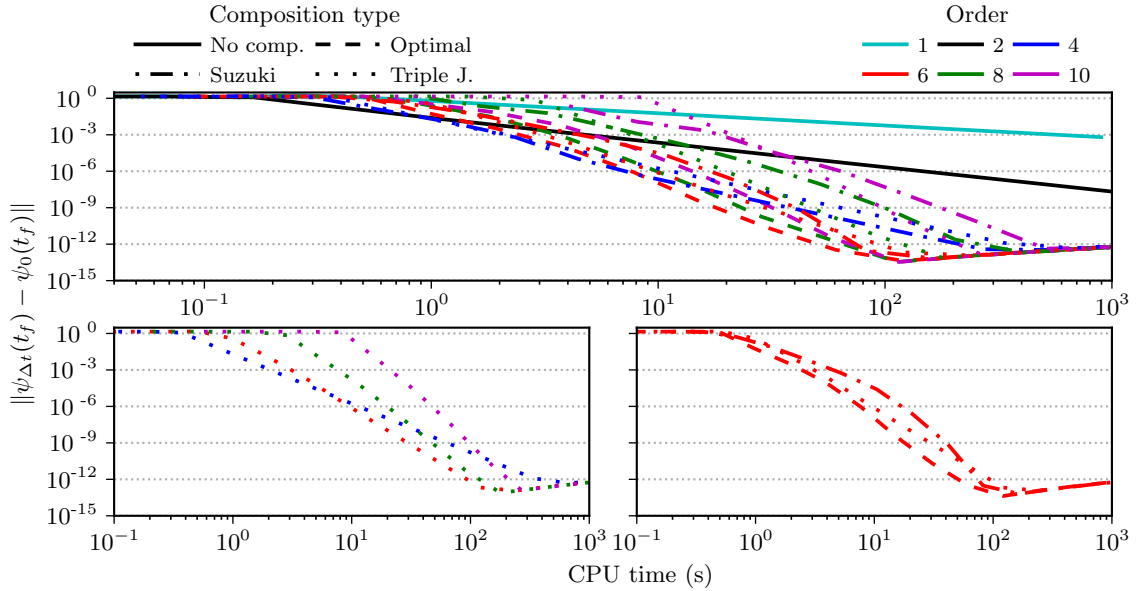


FIG. 5. Efficiency of various compositions of the VTV algorithm shown using the dependence of the convergence error on the computational (CPU) time. Top: all methods, bottom left: triple-jump compositions, bottom right: sixth-order methods. The reference wavefunction  $\psi_0(t_f)$  was chosen as the most accurate point in Fig. 4, i.e., the wavefunction obtained using the optimal eighth-order composition with a time step  $\Delta t = t_f/2^9$ .

## IV. CONCLUSION

We have described geometric integrators for nonadiabatic quantum dynamics in the diabatic representation, in which the Hamiltonian is separable into a kinetic and potential terms. These integrators are based on recursive symmetric composition of the standard, second-order split operator algorithm, and as a result, are explicit, unconditionally stable and exactly unitary, symplectic, symmetric, and time-reversible. Unlike the original split-operator algorithm, which is only second-order, its recursive symmetric compositions, obtained by repeated applications of the standard algorithm with well chosen time steps, can achieve accuracy of an arbitrary even order in the time step.

We justified all these properties analytically and also demonstrated them numerically on a diabatic two-surface model of NaI photodissociation. Indeed, the higher-order integrators significantly sped up calculations when higher accuracy was required. For example, a 600-fold reduction in the computational time was observed by using higher-order methods compared to the second-order split-operator algorithm in order to achieve a convergence error of  $10^{-10}$ . It is plausible that Chebyshev<sup>71</sup> and short iterative Lanczos schemes<sup>38,39</sup> would

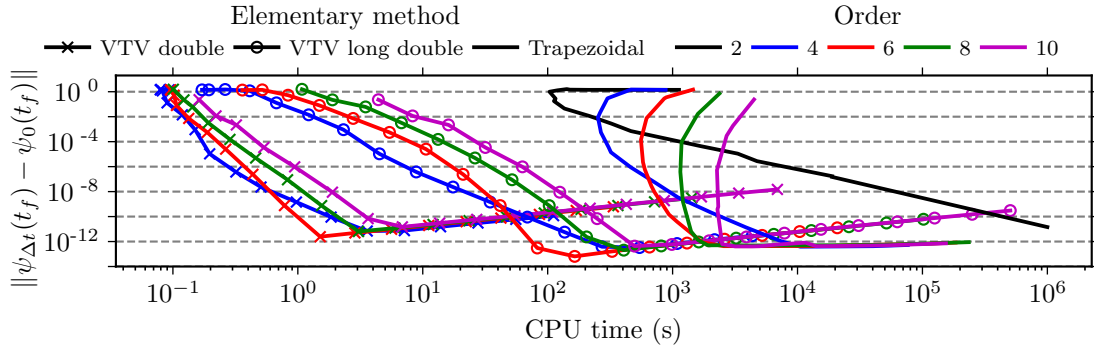


FIG. 6. Efficiency of the Suzuki-fractal compositions of the trapezoidal rule and of the VTV split-operator algorithm. For the trapezoidal rule, only the double precision version of the FFTW3 fast Fourier transform was used, while for the VTV split-operator algorithm, both double and long-double precision versions are compared. The “exact” reference wavefunction  $\psi_0(t_f)$  is the same as in Fig. 5. The result of the elementary second-order trapezoidal rule was extrapolated below the error of  $\approx 10^{-7}$  using the line of best fit; it is the only second-order method shown in order to avoid crowding.

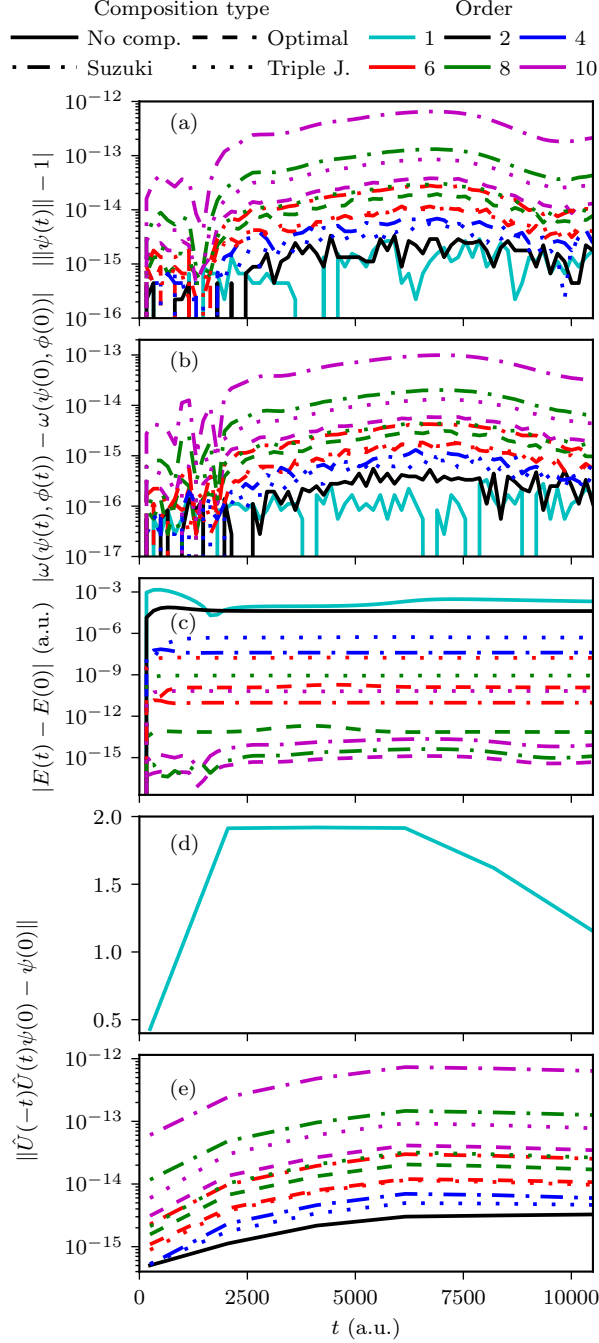


FIG. 7. Conservation of geometric properties by various algorithms: (a) norm, (b) symplectic two-form, (c) energy, and (d)-(e) time reversibility.  $\phi(0)$  is a Gaussian wavepacket with  $q_0 = 5.05$  a.u.,  $p_0 = 2.5$  a.u., and  $\sigma_0$  identical to that of  $\psi(0)$ . Time reversibility was measured by the distance of the initial state  $\psi(0)$  from a forward-backward propagated state, i.e., the state  $\psi(0)$  propagated first forward in time for time  $t$  and then backward in time for time  $t$ . Time step  $\Delta t = t_f/2^7$  a.u. was used in all calculations.

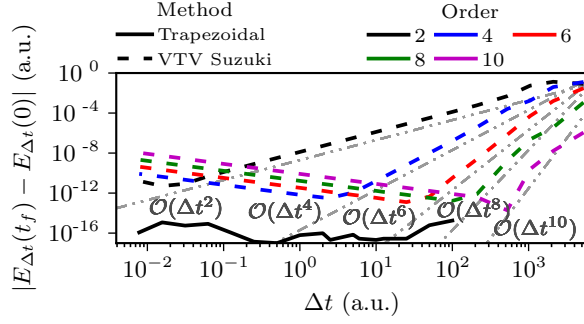


FIG. 8. Energy conservation as a function of the time step.

have comparable efficiency in this and other typical chemical systems, but these methods do not preserve exactly all the geometric properties that are preserved by the compositions of the split-operator algorithms.

The authors acknowledge the financial support from the European Research Council (ERC) under the European Union’s Horizon 2020 research and innovation programme (grant agreement No. 683069 – MOLEQULE).

## Appendix A: Geometric properties of various integrators

To shorten various expressions, we set  $\hbar = 1$  and denote the increment  $\Delta t$  with  $\epsilon$  throughout the Appendix. The  $\hbar$  can be reintroduced by replacing each occurrence of  $t$  with  $t/\hbar$  (and  $\epsilon$  with  $\epsilon/\hbar$ ). To analyze geometric properties of various integrators, we will use the following operator identities:

Let  $\hat{A}$  and  $\hat{B}$  be invertible operators on a Hilbert space, and let  $\hat{A}^\dagger$  and  $\hat{B}^\dagger$  their Hermitian adjoints. Then both  $\hat{A}^\dagger$  and  $\hat{A}\hat{B}$  are invertible, and the following equalities are satisfied:

$$(\hat{A}^\dagger)^{-1} = (\hat{A}^{-1})^\dagger, \quad (\text{A1})$$

$$(\hat{A}\hat{B})^{-1} = \hat{B}^{-1}\hat{A}^{-1}, \quad (\text{A2})$$

$$(\hat{A}\hat{B})^\dagger = \hat{B}^\dagger\hat{A}^\dagger, \quad (\text{A3})$$

$$(\hat{A}^\dagger)^\dagger = (\hat{A}^{-1})^{-1} = \hat{A}. \quad (\text{A4})$$

These properties express that the inverse and Hermitian adjoint operations are compatible involutive antiautomorphisms on the group of invertible operators. The proofs in finite-dimensional spaces can be found in most linear algebra textbooks;<sup>56</sup> the proofs in infinite-

dimensional spaces are given in textbooks on advanced linear algebra or functional analysis.<sup>72</sup>

## 1. Local error

The local error of an approximate evolution operator, defined as  $\hat{U}_{\text{appr}}(\epsilon) - \hat{U}(\epsilon)$ , is typically analyzed by comparing the Taylor expansion of  $\hat{U}_{\text{appr}}(\epsilon)$  with the Taylor expansion of the exact evolution operator:

$$\hat{U}_{\text{ex}}(\epsilon) = 1 - i\epsilon(\hat{T} + \hat{V}) - \frac{1}{2}\epsilon^2(\hat{T} + \hat{V})^2 + \mathcal{O}(\epsilon^3) \quad (\text{A5})$$

If the local error is  $\mathcal{O}(\epsilon^{n+1})$ , the method is said to be of order  $n$  because the global error for a finite time  $t = P\epsilon$  is  $\mathcal{O}(\epsilon^n)$ .

The Taylor expansion of the TV algorithm (14) is

$$\begin{aligned} \hat{U}_{\text{TV}}(\epsilon) &= \left(1 - i\epsilon\hat{T} - \frac{1}{2!}\epsilon^2\hat{T}^2\right) \left(1 - i\epsilon\hat{V} - \frac{1}{2!}\epsilon^2\hat{V}^2\right) + \mathcal{O}(\epsilon^3) \\ &= 1 - i\epsilon(\hat{T} + \hat{V}) - \frac{1}{2}\epsilon^2(\hat{T}^2 + 2\hat{T}\hat{V} + \hat{V}^2) + \mathcal{O}(\epsilon^3) \\ &= \hat{U}_{\text{ex}}(\epsilon) + \frac{1}{2}\epsilon^2[\hat{V}, \hat{T}] + \mathcal{O}(\epsilon^3), \end{aligned} \quad (\text{A6})$$

so the leading order local error is  $\epsilon^2[\hat{V}, \hat{T}]/2$ . Likewise, for the VT algorithm (13),

$$\hat{U}_{\text{VT}}(\epsilon) = \hat{U}_{\text{ex}}(\epsilon) - \frac{1}{2}\epsilon^2[\hat{V}, \hat{T}] + \mathcal{O}(\epsilon^3). \quad (\text{A7})$$

The Taylor expansions of the second-order TVT and VTV algorithms are obtained by composing Taylor expansions (A6) and (A7) for time steps  $\epsilon/2$ :

$$\begin{aligned} \hat{U}_{\text{TVT}}(\epsilon) &= \hat{U}_{\text{VTV}}(\epsilon) = \hat{U}_{\text{ex}}\left(\frac{\epsilon}{2}\right) \hat{U}_{\text{ex}}\left(\frac{\epsilon}{2}\right) + \frac{1}{8}\epsilon^2\left([\hat{V}, \hat{T}] - [\hat{V}, \hat{T}]\right) + \mathcal{O}(\epsilon^3) \\ &= \hat{U}_{\text{ex}}(\epsilon) + \mathcal{O}(\epsilon^3), \end{aligned} \quad (\text{A8})$$

demonstrating that both TVT and VTV are second-order algorithms.

## 2. Unitarity, symplecticity, and stability

Both first-order split-operator algorithms are unitary because

$$\begin{aligned} \hat{U}_{\text{TV}}(\epsilon)^{-1} &= e^{i\epsilon\hat{V}} e^{i\epsilon\hat{T}} = \hat{U}_{\text{TV}}(\epsilon)^\dagger, \\ \hat{U}_{\text{VT}}(\epsilon)^{-1} &= e^{i\epsilon\hat{T}} e^{i\epsilon\hat{V}} = \hat{U}_{\text{VT}}(\epsilon)^\dagger. \end{aligned}$$

Both second-order split-operator algorithms are unitary because they are compositions of unitary first-order algorithms.

Because the symplectic form was defined in Eq. (5) as the imaginary part of the inner product and because VT, TV, VTV, and TVT algorithms as well as their compositions are unitary, all of them are also symplectic.

Stability follows from unitarity because

$$\|\psi(t + \epsilon) - \phi(t + \epsilon)\| = \|\psi(t) - \phi(t)\| \quad (\text{A9})$$

for unitary evolution operator  $\hat{U}_{\text{appr}}(\epsilon)$ . Since all split-operator methods are unitary, all are stable as well.

### 3. Commutation of the evolution operator with the Hamiltonian and conservation of energy

Because the kinetic and potential energy operators do not commute, unless  $\hat{V} = \text{const}$ , the evolution operator of no split-operator algorithm commutes with the Hamiltonian. E.g., for the TV algorithm,

$$[\hat{H}, \hat{U}_{\text{TV}}(\epsilon)] = [\hat{T} + \hat{V}, e^{-i\epsilon\hat{T}} e^{-i\epsilon\hat{V}}] = e^{-i\epsilon\hat{T}} [\hat{T}, e^{-i\epsilon\hat{V}}] + [\hat{V}, e^{-i\epsilon\hat{T}}] e^{-i\epsilon\hat{V}} \neq 0. \quad (\text{A10})$$

As a consequence, no split-operator algorithm conserves energy.

### 4. Symmetry and time reversibility

The adjoint of an evolution operator satisfies the following properties:

$$(\hat{U}(\epsilon)^*)^* = \hat{U}(\epsilon), \quad (\text{A11})$$

$$(\hat{U}_1(\epsilon)\hat{U}_2(\epsilon))^* = \hat{U}_2(\epsilon)^*\hat{U}_1(\epsilon)^*, \quad (\text{A12})$$

$$\hat{U}(\epsilon)\hat{U}(\epsilon)^* \text{ is symmetric.} \quad (\text{A13})$$

The first two properties imply that the adjoint operation  $*$  is an involutive antiautomorphism on the group of invertible operators, whereas the third property gives a simple recipe for constructing a symmetric method—by composing an arbitrary method with its adjoint, with both composition coefficients of  $1/2$ . For the proof, see Appendix A of Ref. 52.



The first-order VT and TV split-operator algorithms are adjoints of each other because

$$\hat{U}_{\text{TV}}(-\epsilon)^{-1} = e^{-i\epsilon\hat{V}}e^{-i\epsilon\hat{T}} = \hat{U}_{\text{VT}}(\epsilon) \quad (\text{A14})$$

and using Eq. (A11). Therefore, neither method is symmetric. In contrast, the second-order VTV and TVT algorithms are both symmetric, which follows from Eq. (A13) applied to the two possible compositions of the VT and TV algorithms with composition coefficients  $1/2$ .

For an elementary time step  $\epsilon$ , time reversibility follows from symmetry because

$$\hat{U}(-\epsilon)\hat{U}(\epsilon) = \hat{U}(-\epsilon)\hat{U}(-\epsilon)^{-1} = 1 \quad (\text{A15})$$

if  $\hat{U}(-\epsilon)^{-1} = \hat{U}(\epsilon)$ . By induction, this argument can be extended to a forward propagation for  $P$  steps followed by a backward propagation for  $P$  steps:

$$\hat{U}(-\epsilon)^P\hat{U}(\epsilon)^P = 1.$$

As a result, neither first-order split-operator method is time-reversible, whereas both second-order methods are.

## Appendix B: Exponential convergence with grid density

Figure 9 exhibits the exponential convergence of the molecular wavefunction with the increasing number of grid points. The ranges as well as the densities of both the position and momentum grids were increased by a factor of  $\sqrt{2}$  for each increase in the number of grid points by a factor of two. Convergence error required comparing wavefunctions on grids with different densities, which was carried out by trigonometric interpolation of the wavefunction on the sparser grid.

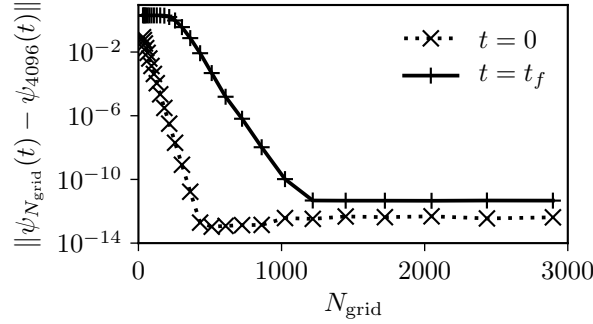


FIG. 9. Convergence of the initial and final wavepackets with the increasing number of grid points. The second-order split-operator VTV algorithm with time step  $\Delta t = t_f/2^7$  was used for propagation.

## REFERENCES

- <sup>1</sup>M. Born and R. Oppenheimer, Ann. Phys. **389**, 457 (1927).
- <sup>2</sup>E. J. Heller, *The semiclassical way to dynamics and spectroscopy* (Princeton University Press, Princeton, NJ, 2018).
- <sup>3</sup>A. Mokhtari, P. Cong, J. L. Herek, and A. H. Zewail, Nature **348**, 225 (1990).
- <sup>4</sup>M. Baer, *Beyond Born-Oppenheimer: Electronic Nonadiabatic Coupling Terms and Conical Intersections*, 1st ed. (Wiley, 2006).
- <sup>5</sup>H. Nakamura, *Nonadiabatic Transition: Concepts, Basic Theories and Applications*, 2nd ed. (World Scientific Publishing Company, 2012).
- <sup>6</sup>K. Takatsuka, T. Yonehara, K. Hanasaki, and Y. Arasaki, *Chemical Theory Beyond the Born-Oppenheimer Paradigm: Nonadiabatic Electronic and Nuclear Dynamics in Chemical Reactions* (World Scientific, Singapore, 2015).
- <sup>7</sup>M. P. Bircher, E. Liberatore, N. J. Browning, S. Brickel, C. Hofmann, A. Patoz, O. T. Unke, T. Zimmermann, M. Chergui, P. Hamm, U. Keller, M. Meuwly, H. J. Woerner, J. Vaníček, and U. Rothlisberger, Struct. Dyn. **4**, 061510 (2017).
- <sup>8</sup>S. Shin and H. Metiu, J. Chem. Phys. **102**, 9285 (1995).
- <sup>9</sup>J. Albert, D. Kaiser, and V. Engel, J. Chem. Phys. **144**, 171103 (2016).
- <sup>10</sup>E. Mátyus, Mol. Phys. **117**, 590 (2019).
- <sup>11</sup>A. Abedi, N. T. Maitra, and E. K. Gross, Phys. Rev. Lett. **105**, 123002 (2010).
- <sup>12</sup>L. S. Cederbaum, J. Chem. Phys. **128**, 124101 (2008).

- <sup>13</sup>T. Zimmermann and J. Vaníček, J. Chem. Phys. **132**, 241101 (2010).
- <sup>14</sup>T. Zimmermann and J. Vaníček, J. Chem. Phys. **136**, 094106 (2012).
- <sup>15</sup>M. Ben-Nun, J. Quenneville, and T. J. Martínez, J. Phys. Chem. A **104**, 5161 (2000).
- <sup>16</sup>B. F. E. Curchod and T. J. Martínez, Chem. Rev. **118**, 3305 (2018).
- <sup>17</sup>D. V. Shalashilin and M. S. Child, J. Chem. Phys. **115**, 5367 (2001).
- <sup>18</sup>D. V. Makhov, C. Symonds, S. Fernandez-Alberti, and D. V. Shalashilin, Chem. Phys. **493**, 200 (2017).
- <sup>19</sup>G. A. Worth, M. A. Robb, and I. Burghardt, Faraday Discuss. **127**, 307 (2004).
- <sup>20</sup>G. Richings, I. Polyak, K. Spinlove, G. Worth, I. Burghardt, and B. Lasorne, Int. Rev. Phys. Chem. **34**, 269 (2015).
- <sup>21</sup>H.-D. Meyer, U. Manthe, and L. S. Cederbaum, Chem. Phys. Lett. **165**, 73 (1990).
- <sup>22</sup>G. A. Worth, H.-D. Meyer, H. Köppel, L. S. Cederbaum, and I. Burghardt, Int. Rev. Phys. Chem. **27**, 569 (2008).
- <sup>23</sup>H. Wang and M. Thoss, J. Chem. Phys. **119**, 1289 (2003).
- <sup>24</sup>G. Avila and T. Carrington Jr, J. Chem. Phys. **147**, 144102 (2017).
- <sup>25</sup>C. Lubich, *From Quantum to Classical Molecular Dynamics: Reduced Models and Numerical Analysis*, 12th ed. (European Mathematical Society, 2008).
- <sup>26</sup>R. Kosloff, J. Phys. Chem. **92**, 2087 (1988).
- <sup>27</sup>G. A. Worth and L. S. Cederbaum, Annu. Rev. Phys. Chem. **55**, 127 (2004).
- <sup>28</sup>W. Domcke and D. R. Yarkony, Annu. Rev. Phys. Chem. **63**, 325 (2012).
- <sup>29</sup>G. Granucci, M. Persico, and A. Toniolo, J. Chem. Phys. **114**, 10608 (2001).
- <sup>30</sup>H. Nakamura and D. G. Truhlar, J. Chem. Phys. **117**, 5576 (2002).
- <sup>31</sup>M. Baer, Phys. Rep. **358**, 75 (2002).
- <sup>32</sup>H. Koppel, W. Domcke, and L. S. Cederbaum, Adv. Chem. Phys. **57**, 59 (1984).
- <sup>33</sup>M. D. Feit, J. A. Fleck, Jr., and A. Steiger, J. Comp. Phys. **47**, 412 (1982).
- <sup>34</sup>D. J. Tannor, *Introduction to Quantum Mechanics: A Time-Dependent Perspective* (University Science Books, Sausalito, 2007).
- <sup>35</sup>E. Hairer, C. Lubich, and G. Wanner, *Geometric Numerical Integration: Structure-Preserving Algorithms for Ordinary Differential Equations* (Springer Berlin Heidelberg New York, 2006).
- <sup>36</sup>L. Verlet, Phys. Rev. **159**, 98 (1967).

- <sup>37</sup>D. Frenkel and B. Smit, *Understanding molecular simulation*, 2nd ed. (Academic Press, 2002).
- <sup>38</sup>C. Lanczos, J. Res. Nat. Bur. Stand. **45**, 255 (1950).
- <sup>39</sup>T. J. Park and J. C. Light, J. Chem. Phys. **85**, 5870 (1986).
- <sup>40</sup>A. I. Kuleff, J. Breidbach, and L. S. Cederbaum, J. Chem. Phys. **123**, 044111 (2005).
- <sup>41</sup>E. Forest and R. D. Ruth, Physica D **43**, 105 (1990).
- <sup>42</sup>M. Suzuki, Phys. Lett. A **146**, 319 (1990).
- <sup>43</sup>H. Yoshida, Phys. Lett. A **150**, 262 (1990).
- <sup>44</sup>A. D. Bandrauk and H. Shen, Chem. Phys. Lett. **176**, 428 (1991).
- <sup>45</sup>A. D. Bandrauk, E. Dehghanian, and H. Lu, Chem. Phys. Lett. **419**, 346 (2006).
- <sup>46</sup>T. Prosen and I. Pižorn, J. Phys. A **39**, 5957 (2006).
- <sup>47</sup>H. De Raedt, Comput. Phys. Rep. **7**, 1 (1987).
- <sup>48</sup>M. Suzuki, Phys. Lett. A **201**, 425 (1995).
- <sup>49</sup>S. A. Chin and C. R. Chen, J. Chem. Phys. **117**, 1409 (2002).
- <sup>50</sup>R. I. McLachlan, SIAM J. Sci. Comput. **16**, 151 (1995).
- <sup>51</sup>M. Wehrle, M. Šulc, and J. Vaníček, Chimia **65**, 334 (2011).
- <sup>52</sup>S. Choi and J. Vaníček, Unpublished.
- <sup>53</sup>J. Crank and P. Nicolson, Math. Proc. Camb. Phil. Soc. **43**, 50 (1947).
- <sup>54</sup>E. A. McCullough, Jr. and R. E. Wyatt, J. Chem. Phys. **54**, 3578 (1971).
- <sup>55</sup>V. Engel and H. Metiu, J. Chem. Phys. **90**, 6116 (1989).
- <sup>56</sup>P. R. Halmos, *Finite dimensional vector spaces* (Princeton University Press, 1942).
- <sup>57</sup>J. Auslander, N. Bhatia, and P. Seibert, Bol. Soc. Mat. Mex. **9**, 55 (1964).
- <sup>58</sup>B. Leimkuhler and S. Reich, *Simulating Hamiltonian Dynamics* (Cambridge University Press, 2004).
- <sup>59</sup>N. P. Bhatia and G. P. Szegő, *Dynamical systems: stability theory and applications*, Vol. 35 (Springer, 2006).
- <sup>60</sup>M. Creutz and A. Gocksch, Phys. Rev. Lett. **63**, 9 (1989).
- <sup>61</sup>W. Kahan and R.-C. Li, Math. Comput. **66**, 1089 (1997).
- <sup>62</sup>M. Sofroniou and G. Spaletta, Optim. Method Softw. **20**, 597 (2005).
- <sup>63</sup>H. F. Trotter, Proc. Amer. Math. Soc. **10**, 545 (1959).
- <sup>64</sup>G. Strang, SIAM J. Numer. Anal. **5**, 506 (1968).
- <sup>65</sup>R. Kosloff and D. Kosloff, J. Chem. Phys. **79**, 1823 (1983).

- <sup>66</sup>D. Kosloff and R. Kosloff, J. Comp. Phys. **52**, 35 (1983).
- <sup>67</sup>M. Frigo and S. G. Johnson, Proc. IEEE **93**, 216 (2005).
- <sup>68</sup>G. H. Golub and C. F. Van Loan, *Matrix Computations*, 3rd ed. (The Johns Hopkins University Press, 1996).
- <sup>69</sup>R. B. Sidje, ACM Trans. Math. Softw. **24**, 130 (1998).
- <sup>70</sup>E. Anderson, Z. Bai, C. Bischof, S. Blackford, J. Demmel, J. Dongarra, J. Du Croz, A. Greenbaum, S. Hammarling, A. McKenney, and D. Sorensen, *LAPACK Users' Guide*, 3rd ed. (Society for Industrial and Applied Mathematics, 1999).
- <sup>71</sup>H. Tal-Ezer and R. Kosloff, J. Chem. Phys. **81**, 3967 (1984).
- <sup>72</sup>P. R. Halmos, *Introduction to Hilbert space and the theory of spectral multiplicity* (Chelsea, 1951).